Chemical Methodologies

Journal homepage: http://chemmethod.com

Original Article

Experimental and Theoretical Study on the Mechanism and Kinetics of the Reaction between Hexamethyl Phosphorous Triamide and Dialkyl Acetylenedicarboxylates in the Presence of Benzimidazole

Younes Ghalandarzehi*[1], Halime Kord-Tamandani[2]

[1] *Faculty of Industry & Mining (Khash), University of Sistan and Baluchestan, P O Box 98135-674, Zahedan, Iran*
[2]*Department of Chemistry, Faculty of Science, University of Sistan and Baluchestan, P O Box 98135-674, Zahedan, Iran*

ARTICLE INFO

Article history
Submitted: 2023-08-20
Revised: 2023-10-04
Accepted: 2023-10-29
Manuscript ID: CHEMM-2308-1714
Checked for Plagiarism: Yes
Language Editor:
Dr. Fatimah Ramezani
Editor who approved publication:
Dr. Elham Ezzatzadeh

DOI:10.48309/chemm.2023.412486.1714

KEYWORDS
Kinetic parameters
UV-Vis spectrophotometery
Theoretical kinetics
Hexamethyl phosphorous Triamide
Dynamic ^{1}H-NMR

ABSTRACT

The study examined the reactions of hexamethyl phosphorous triamide (HMPA) **1**, dialkyl acetylenedicarboxylates **2**, and benzimidazole **3** (NH-acids) by conducting comprehensive kinetic analyses. Kinetics and mechanistic analysis of the reaction were investigated using theoretical and experimental methods. UV-Vis technique was employed to track experimental data whereas ab initio was employed to investigate theoretical studies revolving around the carbon-carbon double bond (OCH_3-C≡C-P $(NMe_2)_3$) in phosphorus ylides **4a-b**. Using UV-Vis spectrophotometry, the second-order fits were automatically drawn, and the second-order rate constants (k_2) were computed by the standard equations within the program. Calculations were made for the reaction's activation energy and parameters (E_a, $\Delta H^{\#}$, $\Delta S^{\#}$ and $\Delta G^{\#}$). Likewise, the gathered data on how the solvent, reactant structure, and reactant concentration affected reaction rates. The suggested mechanism was verified through experimental data and the steady state approximation, the rate-determining step (RDS) found to be the first and the third steps (k_2 and k_3). Three proposed mechanisms were hypothesized through quantum mechanical calculations. However, the second and the third mechanisms did not match with the experimental data, while the first mechanism showed agreement between theoretical and experimental kinetic data. It was found that the HF/6-31G (d, p) basis set provided more accurate results for compound **4a** than the B3LYP/6-31G (d, p) basis set did, whereas the latter performed better for compound **4b**.

* Corresponding author: Younes Ghalandarzehi
E-mail: younes.ghalandarzehi50@gmail.com

GRAPHICAL ABSTRACT

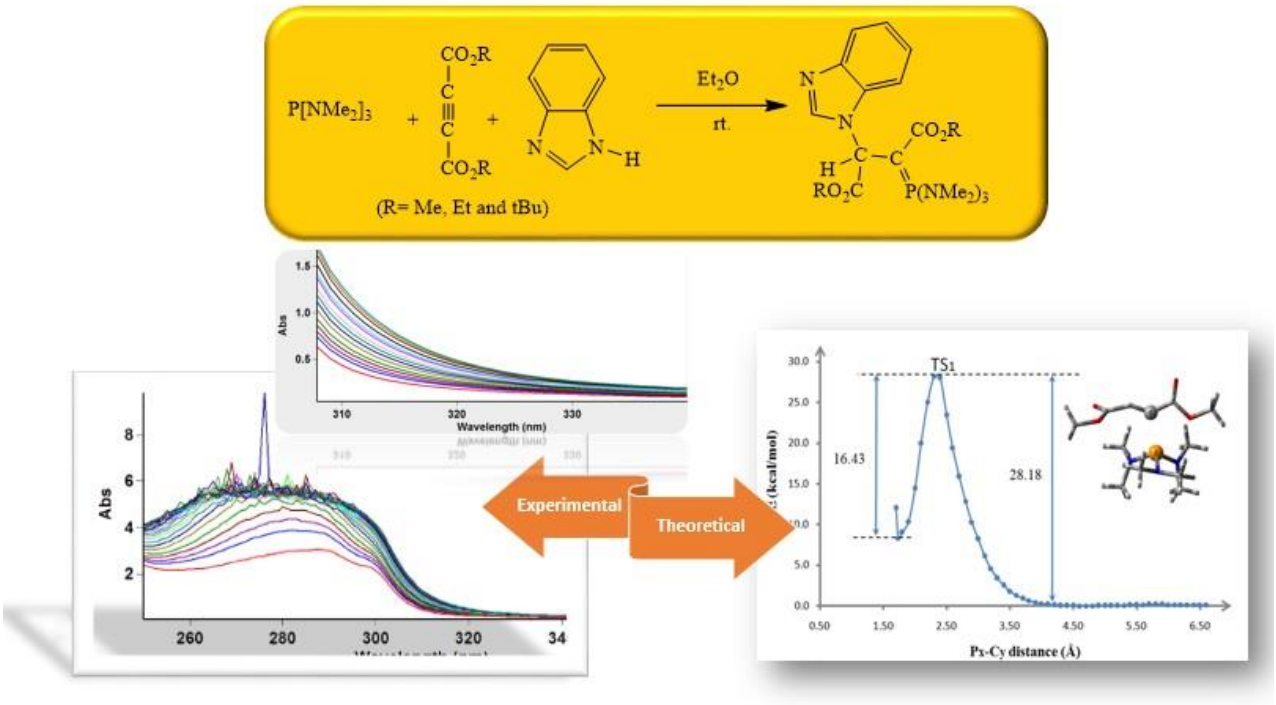

Introduction

The benzimidazole nucleus holds significant importance in the field of drug discovery. Benzimidazole derivatives possess distinctive medicinal properties such as anti-tumor [1, 2], anti-Parkinson [3], antimicrobial [4], and anti-HCV NS3/NS4A serine protease [5] activities. Furthermore, the utilization of benzimidazoles as corrosion inhibitors for metal and alloy surfaces has been widespread [5]. Several metal benzimidazole complexes, namely Chromium (Cr), Manganese (Mn), Iron (Fe), Cobalt (Co), Nickel (Ni), Zinc (Zn), Palladium (Pd), Platinum (Pt), Gold (Au), and Rhenium (Re), have been documented [6-8]. The chemistry field in the 20th century achieved a notable breakthrough with the development of phosphorus ylides [9]. These compounds have proven to be beneficial in numerous reactions that are significant to synthetic chemists, particularly in the production of naturally occurring elements, as well as compounds with biological and pharmaceutical features [10, 11]. Mutilated phosphorus ylides also serve as reducing agents in coordination chemistry and have been extensively used in synthetic chemistry [12-14].

They have gained significant recognition and are often utilized as reagents for connecting synthetic building blocks while creating carbon-to-carbon double bonds and exploring innovative ways to develop heterocyclic systems [15, 16]. These results have significantly raised interest in researching P-ylides and their derivatives synthesis, properties, and structures [17, 18]. Trivalent phosphorus nucleophiles reacting with acetylenic esters alongside O-H, S-H, N-H, or CH-acids have been studied in multiple research topics [19], but in certain circumstances, the ylide commodities cannot be separated, suggesting that they act as intermediates in the reaction pathway before generating the final product [20]. While some of these ylides only contain one isomer, most of them combine the geometric isomers Z and E [21, 22]. Furthermore, some display a dynamic ^{1}H-NMR effect [23-26], which can provide valuable insights into the rotational

isomers' exchangeable process, thereby yielding crucial kinetic data.

We continued our research regarding [26] ylide compounds by conducting a comprehensive investigation that included synthesis, full kinetics analysis, mechanistic investigation, and dynamic ^{1}H-NMR testing.

The study was done in the presence of either triphenylphosphine or triphenyl phosphate. Instead of triphenylphosphine (TPP), we used a bulkier and less reactive hexamethyl phosphorous triamide (HMPA) as a nucleophile to perform similar experiments. Theoretical and experimental methods are used in an analysis of the kinetics and mechanism of the reaction hexamethyl phosphorous triamide **1**, dialkyl acetylendicarboxylate **2**, and benzimidazole 3 was carried out, complemented by theoretical studies that focused on the rotation around the carbon-carbon double bond (C≠C) in a phosphorus ylide. Earlier published data revealed that stable phosphorus ylides with both Z- and E-geometrical isomers could be prepared by synthesizing the reaction between hexamethyl phosphorous triamide, dialkyl acetylendicarboxylate, and N-H acid **3**, and conducting dynamic ^{1}H-NMR studies (Figure 1) [26].

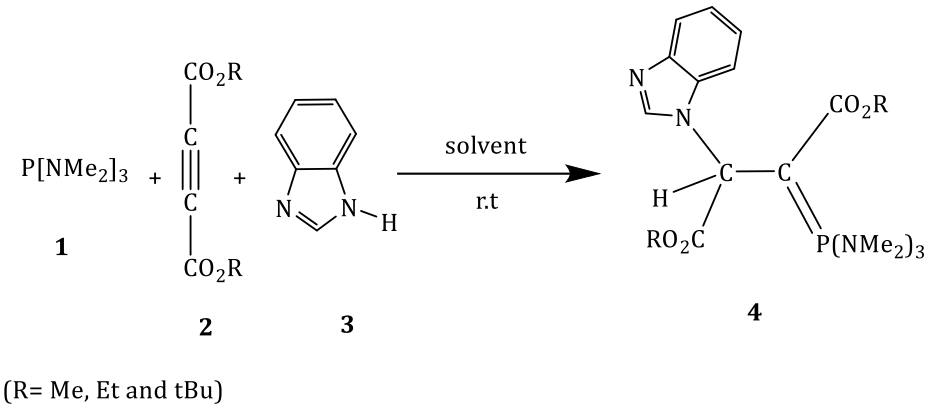

Figure 1: Condensation of stable phosphorus ylides **4**

Experimental

Materials and Instruments

The extra-pure solvents 1,4-dioxane and 1,2-dichloroethane were provided by Merck (Darmstadt, Germany) in addition to the reagents, which were all purchased from Fluka (Buchs, Switzerland). Throughout the current work, reaction spectra and kinetic measurements were made using a Cary UV-Vis spectrophotometer model Bio-300 with a quartz spectrophotometer cell with a 10 mm light path and a thermostated housing cell. Using the GAMESS program, theoretical kinetic studies were conducted [27]. It was assumed that phosphorus ylide **4** (products) was formed from the hexamethyl phosphorous triamide reacting with acetylenic ester **2** (Me, Et, or tBu) followed by protonation of the 1:1 adduct by the NH-acid **3**. The resulting phosphoranes **4** were a product of this reaction. To understand the reaction (HMPA) **1**, dialkyl acetylenedicarboxylates **2**, and benzimidazole 3 to produce stable phosphorus ylides products (Figure 1), the kinetic evaluation was done with a UV-Vis spectrophotometer.[28-32].

Method Kinetics

In the pursuit of identifying the suitable wavelength for monitoring the kinetics of a reaction, an initial experiment was performed. Specifically, a quartz spectrophotometer cell was employed to contain a 1 mL aliquot of the 3×10^{-3} M solutions of each compound of **1** and **3**, as these compounds do not interact, and then the mixture received a 1 mL aliquot of reactant **2** (Me), which is DMAD (dimethyl acetylenedicarboxylates). After that, for the reaction duration at room

temperature, the reaction was monitored and recorded every 7 minutes. In Figure 2, you can see the reaction's UV-Vis spectra. The most suitable wavelength, mainly linked to product **4**, was identified as 320 or 330 nm. Importantly, since compounds **1**, **2** (DMAD), and **3** do not exhibit significant absorbance values at these wavelengths, there was no interference with observing and examining the kinetics utilization and mechanics to study of the reaction between HMPA **1**, **2** (DMAD), and benzimidazole **3**. The absorbance values and compound **4** concentrations were found to be linearly related over the concentration range of ($2\times10^{-4}M \leq M_4 \leq 10^{-3}M$). The following action was taken after choosing the appropriate wavelength and concentration range.

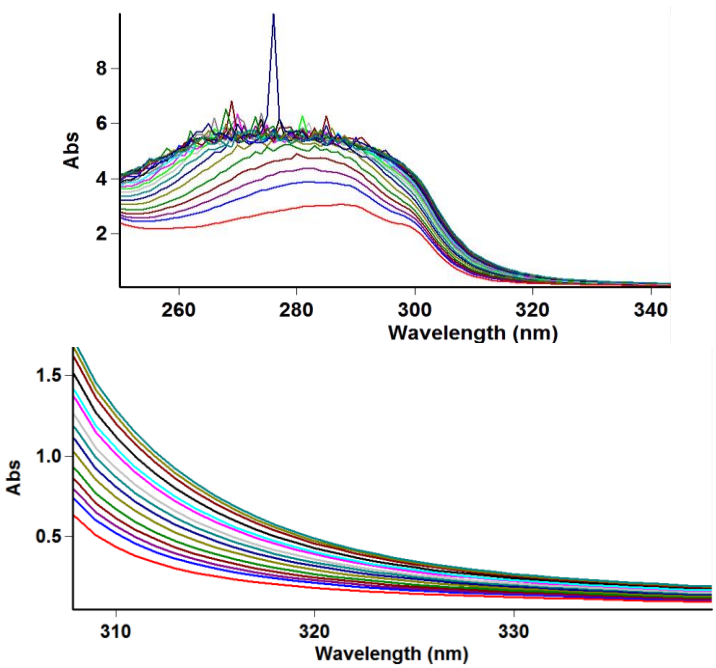

Figure 2: Top: The UV-Vis spectra for the reaction of **1**, **2** (Me), and **3** in 1, 2-dichloroethane for the generation of the product **4**. (Each of concentration compound is $10^{-3}M$). **Bottom:** Expanded section of UV-Vis spectra

The study investigated the kinetics of a 1:1:1 addition reaction between **1**, **2** (Me), and **3** *via* UV-Vis absorbance at 15.0 °C and a wavelength of 330 nm, as depicted in Figure 3, 4. The absorbance at the end of the reaction (A_∞), which was determined from Figure 2 at t=420 min, was shown as a change in absorbance over time on the experimental curve (dotted line). The UV-Vis instrument was used to generate a second-order fit curve based on the original experimental absorbance data, and it was found that it perfectly matched the experimental curve (dotted line). The resulting second-order rate constant (k_2) was calculated using a standard equation [32] within the program, and the values at 15.0 °C were obtained in Tables 1 and 2. Moreover, analogous to the precedent experiment that used concentrations of 5×10^{-3} M and 7×10^{-3} M for each reactant; further experimentation was conducted to investigate the kinetics involved. It was observed that the second-order rate constant remained unchanged, exhibiting independence from the employed reactants concentration. The explicit rate constant value that was measured was equivalent to that obtained in the anterior experiment. Furthermore, the reaction was categorized as following a second-order of reaction based on the experimental data analysis. The experiment data from Tables 1 and 2 are consistent with the results at the two wavelengths λ=320 and 330 nm in Tables 1 and 2, respectively).

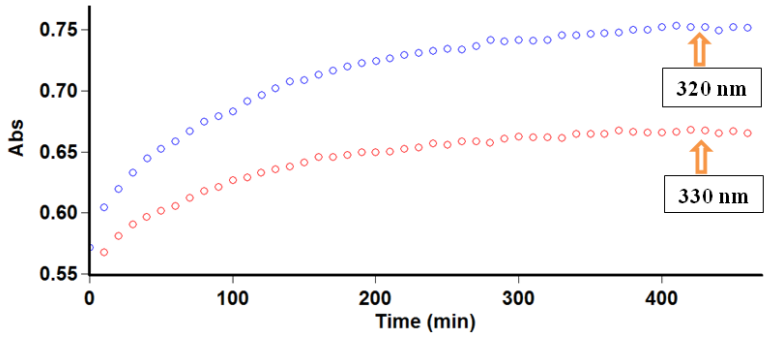

Figure 3: Original experimental absorbance versus time curve (dotted line) related to the reaction of reactant **1**, **2** (Me), and **3** in reacting in 1, 2-dichloroethane (T= 15 °C, λ=320, and 330 nm)

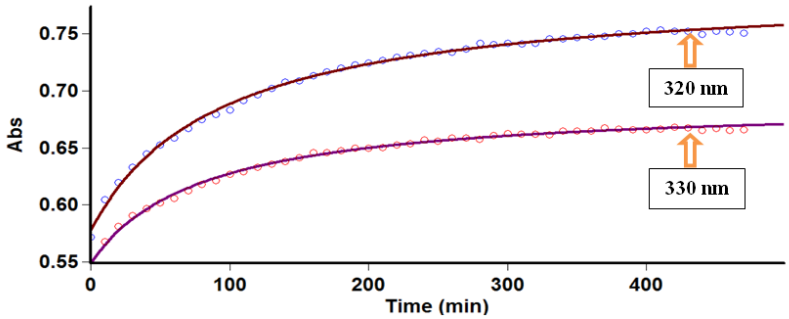

Figure 4: The original experimental curve (dotted line) and second-order fit curve (solid line) related to the reaction of reactant **1**, **2** (Me), and **3** in which proceeded in 1, 2-dichloroethane (T= 15.0 °C, λ=320, and 330 nm)

Table 1: Rate constant (k_{ovr}) values for reactions of **1**, **2** (Me), and **3** (10^{-2} M) at different temperatures and solvents under the same conditions (λ =320 nm)

Reaction	ε	Solvent	k_2.M^{-1}.min^{-1}			
			15.0 °C	20.0 °C	25.0 °C	30.0 °C
1, **2** (Me), and **3**	2.2	1,4-dioxane	1.95	3.02	6.47	11.12
	10.3	1,2-dichloroethane	6.19	13.66	20.74	33.21
1, 2(tBu) and **3**	10.3	1,2-dichloroethane	0.32	0.67	1.07	1.72

Table 2: Rate constant (k_{ovr}) values for reactions of (1), (2), and (3) (10^{-2} M) at different temperatures and solvents under the same conditions (λ =330 nm)

Reaction	ε	Solvent	k_2.M^{-1}.min^{-1}			
			15.0 ºC	20.0 °C	25.0 °C	30.0 °C
1, **2** (Me), and **3**	2.2	1,4-dioxane	1.78	2.65	5.36	10.115
	10.3	1,2-dichloroethane	5.34	12.85	18.90	31.87
1, 2(tBu) and **3**	10.3	1,2-dichloroethane	0.31	0.66	1.05	1.70

Results and Discussion

Temperature and Solvent Effects

This study set out to determine how variations in temperature and solvent environment would impact reaction rate. To achieve this objective, a series of experiments were conducted under varying temperatures and solvent polarities, while keeping all other conditions identical to the previous experiment. To select a suitable solvent, 1, 4-dioxane with a 2.2 dielectric constant was chosen given its ability to dissolve all compounds

without any reaction. Based on the findings, it was observed that the reaction rate increased at higher temperatures in all cases. At all temperatures examined, the rate of reactions involving **1**, **2**(Me), and **3** also increased rather than decreased with a higher dielectric constant environment (1, 2-dichloroethane) compared to a lower dielectric constant environment (1, 4-dioxane). The relationship between the second-order rate constant (Ln K2) and the reciprocal temperature for the studied temperature range was consistent with the Arrhenius equation, from which the activation energy of the reaction was obtained using the slope of Figure 5 (See Table 3).

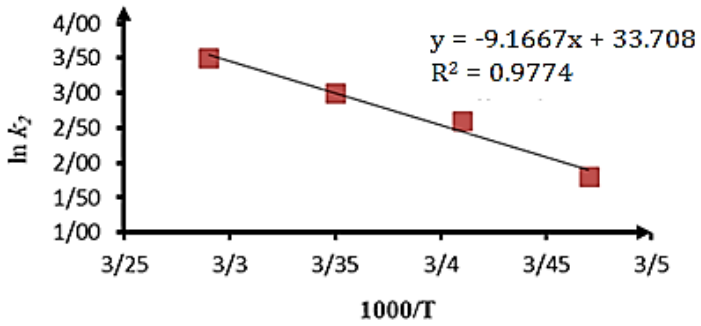

Figure 5: Dependence of the second-order rate constant (Ln k_2) on the reciprocal temperature for the reaction between compounds **1**, **2**(Me), and **3** in 1, 2-dichloroethane, (According to the Arrhenius equation, (λ =320 nm))

Influence of Concentration

To establish the reaction order in relation to **1** and **2** (Me, Et and tBu), an inquiry was pursued by conducting kinetic studies in the presence of an excessive quantity of compound **3**. Due to this circumstance, the rate equation 1 can be written as follows:

$$rate = k_{obs}[1]^{\alpha}[2]^{\beta} \text{ and } k_{obs} = k_2[3]^{\gamma} \qquad (1)$$

In this work, a second-order fit curve (solid line) against time at 320 and 330 nm that precisely matched the experimental curve was obtained using the original experimental absorbance versus time data with a concentration of 3×10^{-2} M rather than 3×10^{-3}M. The resultant rate constant was identical to that which was obtained from the preceding experiment involving a concentration of 3×10^{-3} M. Repetition of the experiments utilizing concentrations of 5×10^{-2} M and 7×10^{-2} M of 3, respectively, gave the same fit curve and rate constant. The experimental findings demonstrated that the pseudo second-order rate constant (k_{obs}) that was observed was equal to the actual second-order rate constant (k_2). This is only possible if the answer to equation 1 is zero. It appears that the reaction is zero and second order, respectively, with regard to **3** (NH-acid) and the result of **1** and **2**, (α + β = 2).

To ascertain the reaction order concerning dialkyl acetylenedicarboxylate **2**, an additional phase of experimentation was carried out accompanied by an excess of 1, with the rate of

$$((\text{rate} = k'_{obs}[3]^{\gamma}[2]^{\beta}, k'_{obs} = k_2[1]^{\alpha}) \qquad (2)$$

The initial absorbance versus time data was utilized to produce a pseudo-first-order fit curve at 320 nm. As demonstrated in Figure 6, the final fit curve (dotted line) perfectly matched the experimental curve.

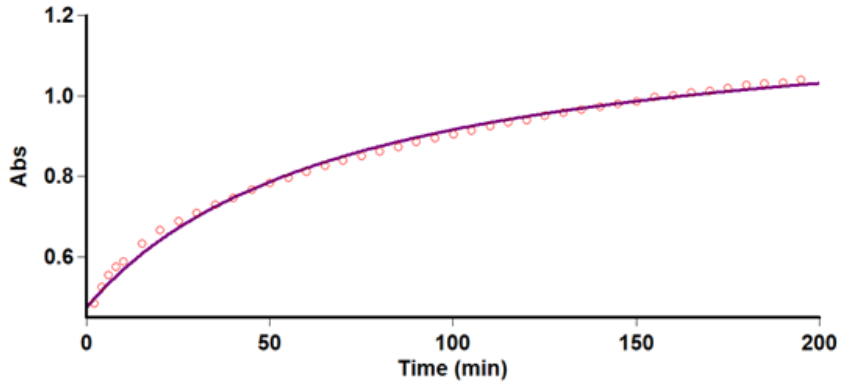

Figure 6: Pseudo first -order fit curve (solid line) the reaction of **2** (Me) and **3** in the presence of excess **1** (10^{-2} M) at 15.0 ˚C in 1, 2-dichloroethane (λ=320 nm)

Consequently, owing to the previously determined value of γ being equal to zero, it is plausible to accept that the reaction conforms with the first-order kinetics concerning compound 2 (DMAD) (where β is equal to one). Since the combined reaction rate order is two (α + β + γ = 2), it is manifest that α must be equal to one and, correspondingly, the order of hexamethyl phosphorous triamide 1 ought to be one. In addition to (**1**, **2**(Me), and **3**), this empirical observation was also determined for the reactions between (**1**, **2**(tBu), and **3**). As illustrated in Figure 7, the results described above lead to a suggested reaction mechanism.

$$1 + 2 \xrightarrow{k_2} I_1$$

$$I_1 \xrightarrow{k_{-2}} 1 + 2$$

$$I_1 + 3 \xrightarrow{k_3} I_2 + N^-$$

$$I_2 + N^- \xrightarrow{k_4} 4$$

Figure 7: A description of the reaction mechanism under consideration.

The results of the experiments suggest that the third step, or the rate constant k_3, may show a significant order of rate. However, it is plausible to hypothesize that this particular step serves as the critical factor that determines the overall rate of the proposed mechanism. If that is indeed the case, the rate law can be articulated in the following manner:

$$rate = k_3[I_1][3] \quad (3)$$

The steady-state assumption can be used for $[I_1]$, which is derived from the previous equation 4:

$$[I_1] = \frac{k_2[HMPA][2]}{k_{-2} + k_3[3]} \quad (4)$$

Equation 5 can be reached by changing the value of $[I_1]$ in Equation 3.

$$rate = \frac{k_2 k_3 [HMPA][2][3]}{k_{-2} + k_3[3]} \quad (5)$$

The following is a reasonable assumption since k3 was previously believed to be important to the RDS: $k_{-2} >> k_3$ [3]
The rate low becomes:

$$rate = \frac{k_2 k_3 [HMPA][2][3]}{k_{-2}} \quad (6)$$

The order of reactions according to Equation 6 is three, which is different from the experimental overall order of reaction, which is two. Furthermore, the equation suggests that the order of reaction concerning benzimidazole 3 is one, whereas it has been proven to be zero. Consequently, it can be inferred that the third step occurs rapidly. Assuming that the rate constant k_4 is the RDS for the proposed mechanism, two ionic species should be considered in the rate determining step: phosphonium ion (I_2) and benzimidazole ion (N^-). As depicted in Figures 7 or 8, phosphonium and benzimidazole ions possess full positive and negative charges and form potent ion-dipole bonds with 1,2-dichloroethane, a solvent with a high dielectric constant. However, the phosphonium and benzimidazole ions that are fighting each other are dispersed in the charge of the transition state for the reaction between the two ions. When compared to the concentrated charge of benzimidazole and phosphonium ions, the bonding of the solvent (1,2-dichloroethane) to this dispersed charge would be much weaker.

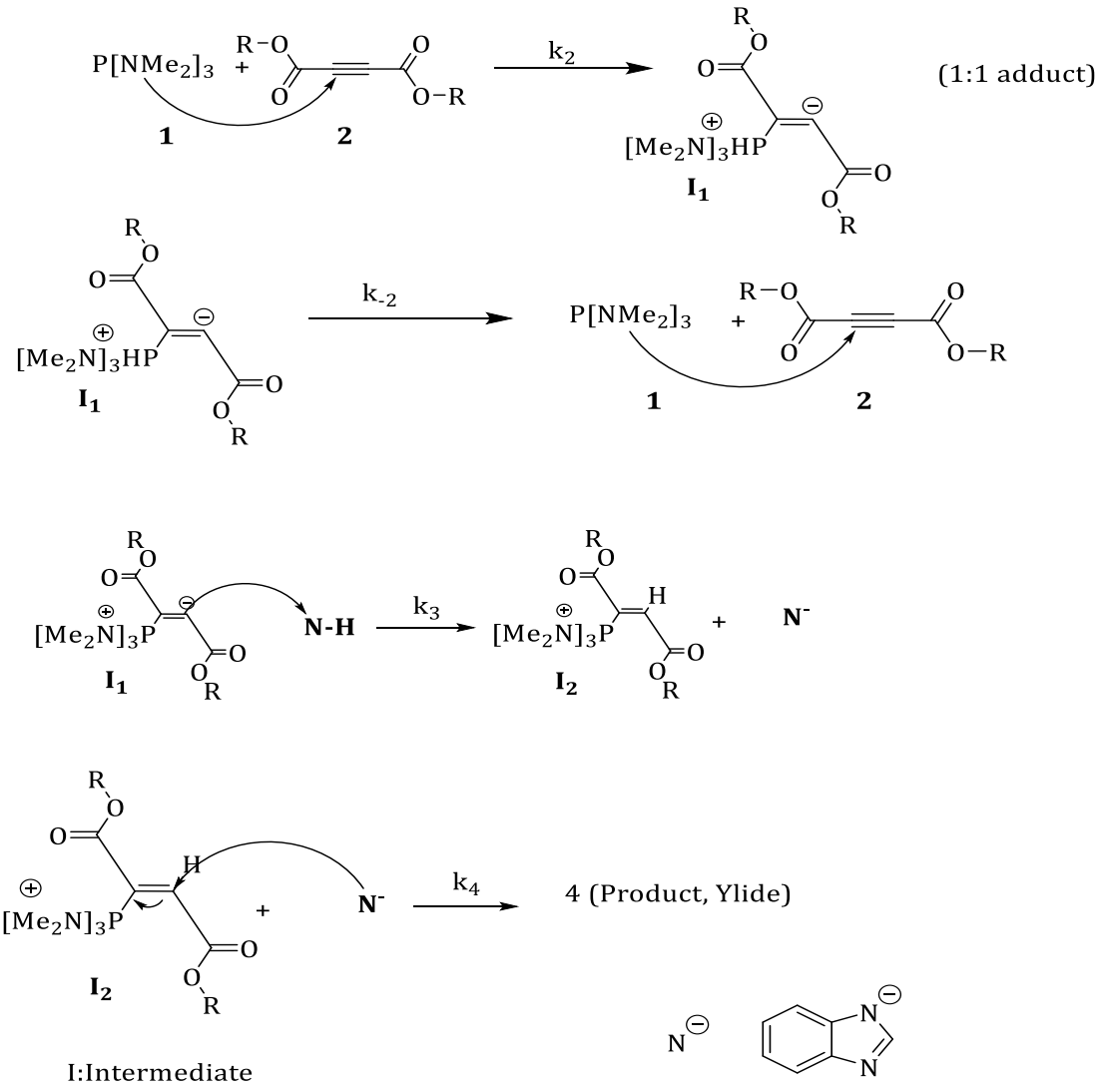

Figure 8: A mechanism of the reactions **1**, **2** (Me, Et, and tBu), and **3** for the synthesis of products phosphorus ylides has been presented

Figures 7 or 8 demonstrate the existence of phosphonium and benzimidazole ions, which possess full positive and negative charges, respectively. These ions form particularly potent ion-dipole bonds to 1,2-dichloroethane, a solvent offering a high dielectric constant. Despite their efficacy, the transition state for the reaction involving the two ions carries a dispersed charge,

divvied up of the attacking benzimidazole and phosphonium ions. This dispersed charge is less strongly bonded to solvent (1, 2-dichloroethane) than are the concentrated charges of benzimidazole and phosphonium ions. As a result, the solvent stabilizes the species ions to a greater extent than the transition state. Consequently, the activation energy (Ea) is elevated, leading to a slower reaction. However, interestingly, in actual experimentation, the reaction is accelerated by 1, 2-dichloroethane (as provided in Tables 1 and 2). Thus, the fourth step of the process, which is independent of the solvent medium, cannot be the rate-determining step. To suggest a reaction mechanism using the steady state assumption, the rate equation governing the creation of the product (the fourth step) can be written as: rate $=k_4\,[I_2]\,[N^-]$.

The resulting equation can be written as follows by applying the steady-state assumption for $[I_2]$ and $[N^-]$ and substituting their values into the over Equation 7:

$$rate=\frac{k_2\,k_3\,[HMPA][2][3]}{k_{-2}+k_3\,[3]} \qquad (7)$$

Changes in the solvent medium do not effect on the fourth step, k_4, since the given equation (7) is independent of the rate constant of this step (k_4). Previous studies have suggested that the kinetics associated with ionic species phenomena, particularly the fourth step, are rapid [33, 34]. If the rate-determining step were the initial step (rate constant k_2), as observed in Figures 7 or 8, the lack of charge on the two reactants, hexamethyl phosphorous triamide 1 and dialkyl acetylenedicarboxylate **2**, would make it impossible for them to form strong ion-dipole bonds with the solvent with a high dielectric constant, such as 1,2-dichloroethane. Due to the transition state's dispersed charges, which are divided between the attacking 1 and 2; a stronger bonding with the solvent than with the reactants is possible. Due to the solvent's superior ability to stabilize the transition state compared to the reactants, this lowers the activation energy Ea and speeds up the reaction. As determined by the results of the experiment, solvents with higher dielectric constants have a significant impact on reaction rate, particularly on the initial step of the proposed mechanism, which has a rate constant of k_2. In contrast, solvents with lower dielectric constants, such as 1, 4-dioxane, exert an opposite effect (refer to Tables 1 and 2). These results collectively provide strong evidence for steps 1, 3, and 4 of the reaction between **1** and **2** (Me, Et, and tBu), and **3**. Although neither of the two steps involving **3** and **4** is determining, the combined effects strongly support the hypothesis that the first step (k_2) of the proposed mechanism is the RDS. The proposed mechanism is often supported by a mechanistic scheme based on the steady-state approximation, which provides a good kinetic description of the experimental results. By employing this technique, the rate of product **4** formation based on the reaction mechanism presented in Figure 8 can be obtained.

$$\frac{d[4]}{dt}=\frac{d[product]}{dt}=rate=k_4\,[I_2][N^-] \qquad (8)$$

The steady-state approximation can be applied to $[I_1]$ and $[I_2]$;

$$\frac{d[I_1]}{dt}=k_2\,[HMPA][2]-k_{-2}\,[I_1]-k_3\,[I_1][3] \qquad (9)$$

$$\frac{d[I_2]}{dt}=k_3\,[I_1][3]-k_4\,[I_2]\,[N^-] \qquad (10)$$

To derive an appropriate expression for $[I_2]$ that can be incorporated into Equation 5, we may postulate that, following an initial transitory phase, the concentrations of $[I_1]$ and $[I_2]$ stabilize at a steady state wherein their rates of formation and disappearance equilibrate. Consequently, both Equations 9 and 10 would equal zero, allowing us to determine expressions for $[I_2]$ and $[I_1]$ using the following Equations 11, 12:

$$[I_2]=\frac{k_3[I_1][3]}{k_4\,[N^-]} \qquad (11)$$

$$[I_1]=\frac{k_2[HMPA][2]}{k_{-2}+k_3[3]} \quad (12)$$

Now that we have the Equation 11 we can replace $[I_1]$ to drive the Equation 13.

$$[I_2]=\frac{k_2\,k_3\,[HMPA][2][3]}{k_4\,[N^-]\left[k_{-2}+k_3\,[3]\right]} \quad (13)$$

By putting the value of $[I_2]$ into Equation 8, the Rate Equation 14 for the suggest mechanism can be obtained:

$$rate=\frac{k_2\,k_3\,k_4[HMPA][2][3][N^-]}{k_4\,[N^-]\left[k_{-2}+k_3\,[3]\right]}$$

or

$$rate=\frac{k_2\,k_3\,[HMPA][2][3]}{\left[k_{-2}+k_3\,[3]\right]} \quad (14)$$

Given that experimental evidence has shown that steps 3 and 4 occur rapidly, whereas step 1 proceeds slowly, the following hypothesis makes sense as a whole:

$k_3\,[3] >> k_{-2}$

As a result, the final equation is:

$$rate=k_2\,[HMPA][2] \quad (15)$$

The equation presented, derived from a mechanistic scheme (illustrated in Figures 7 or 8) using the steady-state approximation, is consistent with the observations gathered through UV-Vis spectrophotometry. Using the Eyring model in terms of Equation 15, which shows the overall reaction rate, it is now possible to calculate the activation parameters for the first step (the RDS and k_2) as an elementary reaction. The results have been tabulated at 298 K and are provided in Table 3.

Table 3: The activation parameters (initial step k_2) for the reactions of (**1**, **2** (Me), and **3**) and (**1**, **2** (tBu), and **3**) in 1, 2-dichloroethane at 298K (λ=320 nm)

Reaction	$\Delta G^{\#}$(kcal.mol^{-1})	$\Delta H^{\#}$(kcal.mol^{-1})	$\Delta S^{\#}$(kcal.mol^{-1}.K^{-1})	*E*a(kcal.mol^{-1})
1, 2(Me) and **3**	19.22	17.83	0.01	2.59
1, 2(tBu) and **3**	19.21	27.03	0.03	6.22

Further kinetic investigations

Additional experiments were conducted to validate the above results using di-tert-butyl acetylenedicarboxylate **2** (tBu) and the same setups used in earlier studies. The second-order rate constant (k_2) values to the reactions involving (**1**, **2**(tBu), and **3**) as well as (**1**, **2**(Me) and **3**) for all the temperatures and solvents examined, as indicated in Tables 1 and 2. The original experimental absorbance curves (dotted line), accompanied by the second-order fit curves (solid line), which perfectly aligned with the experimental curves (dotted line), verify the preceding observations for the new reaction (**1**, **2c**, and **3**) at wavelengths of 320 nm and 330 nm and a temperature of 15.0 °C. As illustrated in Tables 1 and 2, di-*tert*-butyl acetylenedicarboxylate **2** (tBu) displays similar behavior to dimethyl acetylenedicarboxylate **2** (Me) concerning the reaction with hexamethyl phosphorous triamide **1** and benzimidazole **3**. The latter reaction also occurred more quickly in environments with higher temperatures and dielectric constants. However, under the same conditions, these rates are roughly 18 to 20 times lower than those observed for the reaction with dimethyl acetylenedicarboxylate **2** (Me) (typical at 15 °C; Refer to Table 1).

It appears that both the inductive and steric factors associated with the bulky alkyl groups in **2** (tBu) serve to reduce the overall reaction rate (refer to Equation 15). In contrast, the lower steric and inductive effects exerted by the dimethyl groups in dimethyl acetylenedicarboxylate **2**(Me) affect the reaction rate significantly.

Kinetic studies on theory-based

There are several proposed mechanisms for each of the typical organic reactions, each of which has its unique mechanism. However, confirming the mechanism via experimental methods is often limited by instrumental constraints such as the inability to trap intermediates or transition states (TSs). Computational methods offer a more cost-effective and precise means of confirming mechanisms. Here, three theoretical mechanisms were explored for the reaction of **1**, **2** (Me), and N-H acid such as benzimidazole **3** in the gas phase. The aim was to achieve a better understanding of the desired mechanism vis-a-vis the speculative experimental mechanism.

Computation-based methods

The reaction's reactant, product, intermediate (I), and transition state (TS) geometries were all optimized at the HF/6-31G(d,p) [35, 36] level of theory. To account for P and N atoms, an additional 6-31+G(3df,3pd) basis set was included. Harmonic vibrational frequencies were computed to verify their respective species, also at the same level. Static points were categorized as true minima if no fictitious vibrational frequency was present. The imaginary vibrational frequency could be applied to describe transition states. To make sure that reactants, transition states, and products were connected in each step, an intrinsic reaction coordinate (IRC) pathway beginning with the transition states was used [37]. The single-point energy calculation was carried out using the higher-level electronic correlation method B3LYP/6-311 G(d,p) [38, 39], increase the accuracy of the energetic data on the minimum energy path (MEP). The GAMESS program was used to perform all calculations [27]. Given these circumstances, three speculative mechanisms (**1**, **2**, or **3**) are explored below.

Theoretical investigation into the proposed speculative mechanism. No. 1

Theoretical mechanism 1, which is speculative in nature, remains consistent with a proposed joint experimental mechanism (as illustrated in Figure 8).

The aforementioned mechanism is also depicted in Figure 9. The initial step of mechanism 1 (Figure 9), denoted as $step_{1\text{-}1}$, involves the initiation of the reaction via cleavage of the C_y-C_z bond and formation of the P_x-C_y bond. The first transition state ($TS_{1\text{-}1}$, see Figure 10) comprises a C_y-C_z bond distance of 1.21 angstroms and a P_x-C_y bond distance of 2.43 angstroms at the point of bond cleavage and the formation respectively. Based on calculations of vibration frequencies at the HF/6-31G (d,p) level, presented in Table 4, it can be inferred that HMPA, DMAD, and I_1 (dipolar phosphonium ion) represent the genuine minimum points.

It is important to highlight that the TS_1 optimization was conducted at the HF/6-31G (d,p) level and its calculated imaginary frequency (302.12i) confirms that it represents a transition state. During the progression of mechanism 1, specifically in $steps_{1\text{-}2}$ as illustrated in Figure 9, a chemical reaction takes place wherein the dipole phosphonium ion (I_1) and benzimidazole combine to form another intermediate, namely phosphonium ion (I_2), through the formation of a C_z-H bond. The second transition state ($TS_{1\text{-}2}$, depicted in Figure 11) is characterized by a forming C_z-H bond distance of 1.30 angstrom. Notably, $TS_{1\text{-}2}$ exhibits a single imaginary frequency at 1337.89i cm^{-1}, as indicated in Table 4.

During the third step (k_4) of mechanism 1, as displayed in Figure 9, the reaction proceeds between two distinct ionic species, namely phosphonium ion (I_2) and benzimidazole ion, resulting in the production of ylide 4. Despite repeated attempts to identify a transition state (TS) within this particular step, we were unable to do so due to the rapid kinetics exhibited by the ionic species involved. It is significant to note that both the phosphonium and benzimidazole ions collaborate in generating ylide 4. Table 5 presents the activation energies associated with each step of mechanism 1, while the full potential energy profile for the title reaction can be found in Figure 12.

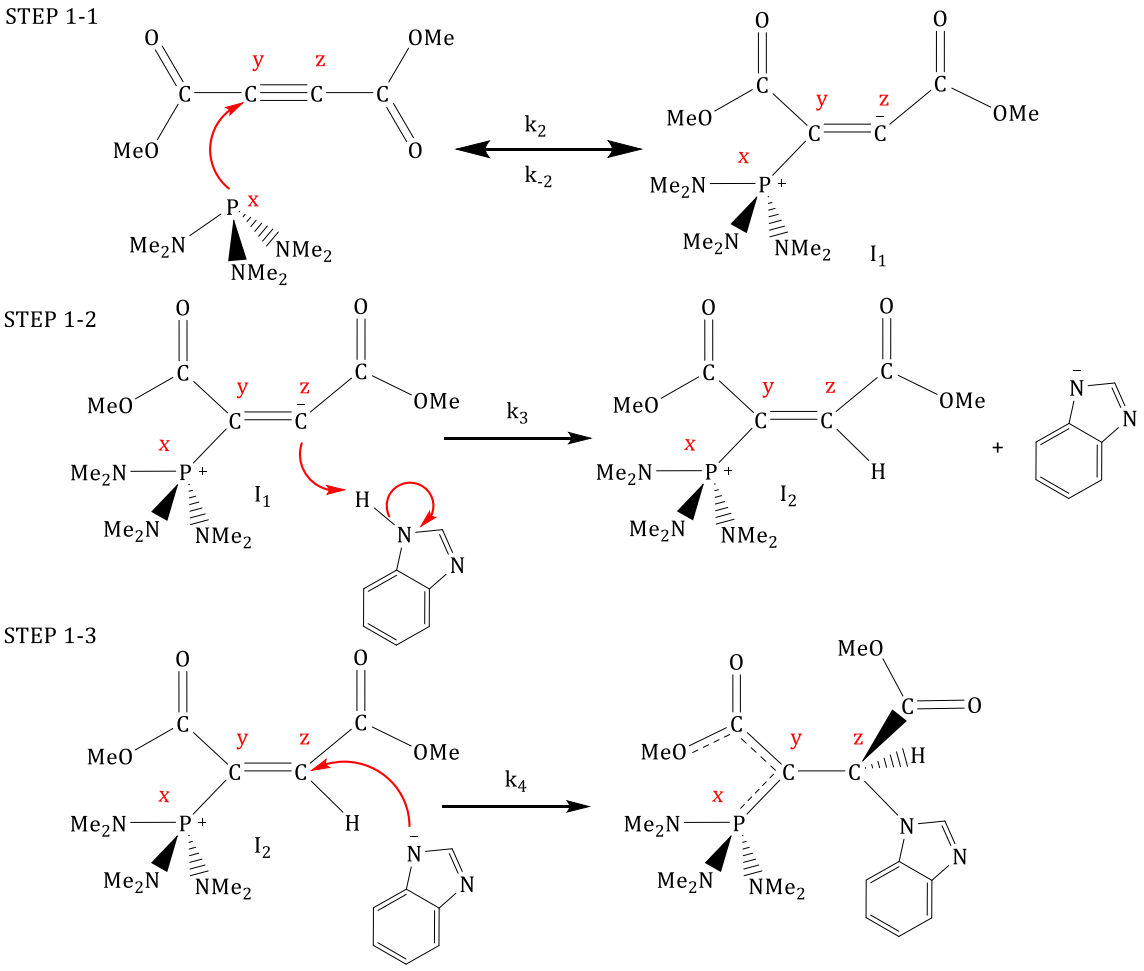

Figure 9: Generation of ylides 4 through three steps: a hypothetical proposed mechanism 1

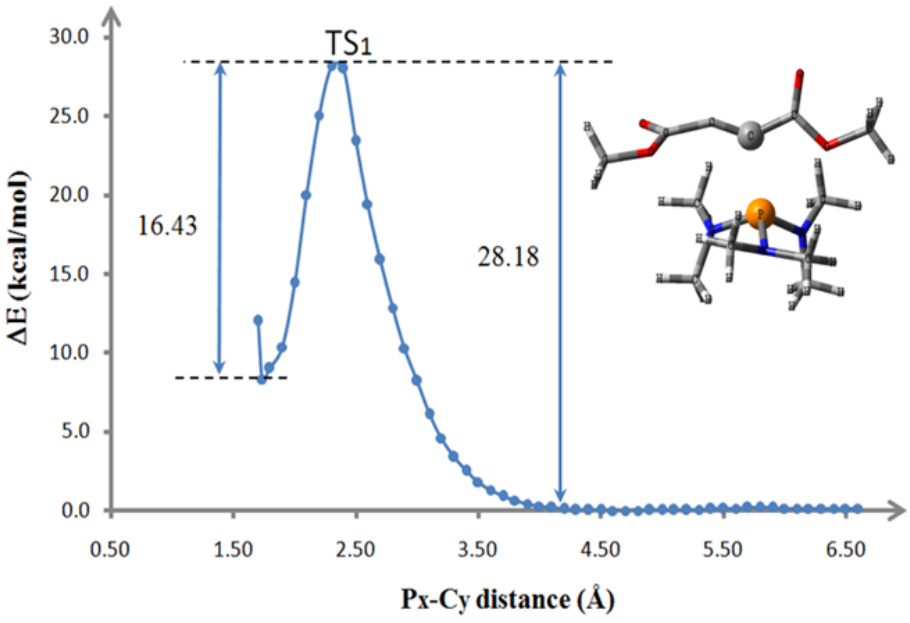

Figure 10: The potential energy profile for the step1-1 of proposed mechanism 1 at HF/6-31G (d,p) [52] level by extra 6-31+G(3df,3pd) basis set for P and N atoms

Table 4: The first stretching frequency for all species (HF/6-31G(d,p) level of theory)

Species *(Mechanism1)*	First stretching frequency
Dimethyl acetylenedicarboxylate (DMAD)	30.88
Hexamethyl phosphorous triamide (HMPA)	28.14
N-H acid benzimidazole	30.11
Ylide 4	10.67
Intermediate I_1	49.37
Intermediate I_2	22.13
TS_1	-302.12
TS_2	-1337.89

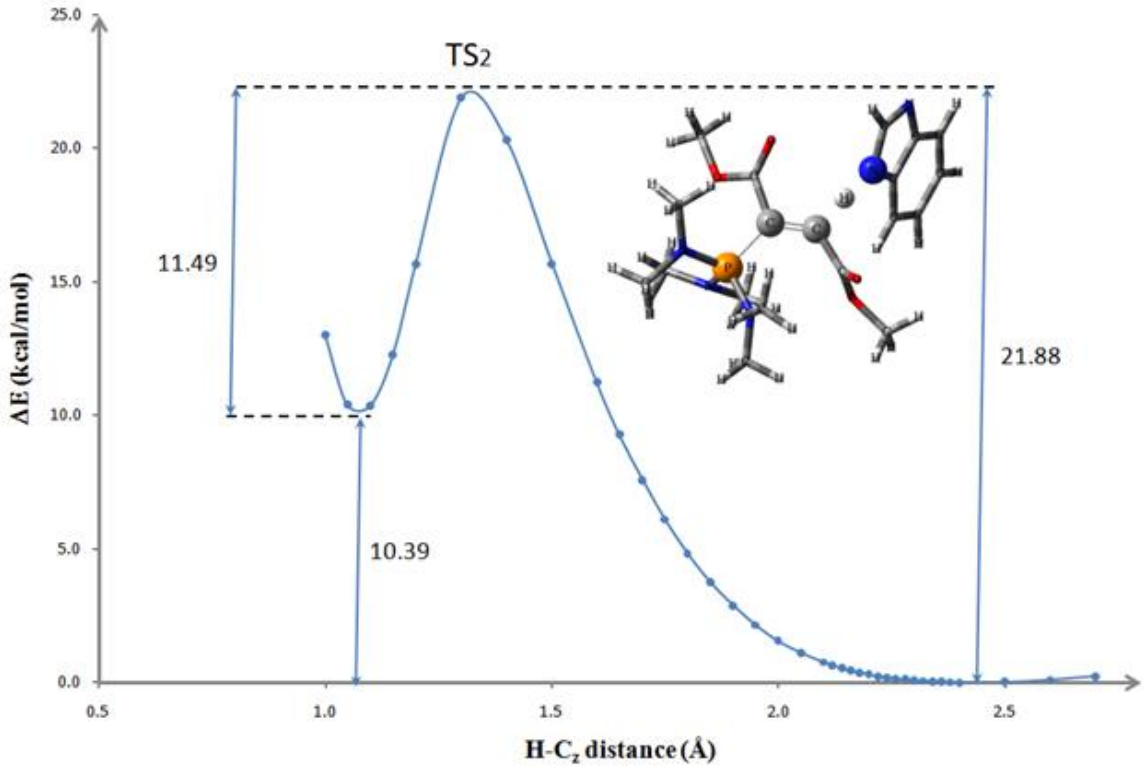

Figure 11: Energy profile for the second step for proposed mechanism 1 at HF/6-31G(d,p) [30] with extra 6-31+G(3df,3pd) basis set for P and N atoms. When the H atom of benzimidazole is gradually brought near to the carbanion (C_z) of intermediate I for generation of intermediate I_2

Table 5: Activation energy for the each steps, HF/6-31G(d,p) level with extra 6-31+G(3df,3pd) basis set for P and N atoms B3LYP/6-311++G(d,p) level

Mechanism 1(steps)	HF/kcal.mol^{-1}	B3LYP/kcal.mol^{-1}
step$_{1\text{-}1}$ (k_2)	28.18	18.58
step$_{1\text{-}2}$ (k_3)	21.88	11.32
step$_{1\text{-}3}$ (k_4)	0.0	0.0

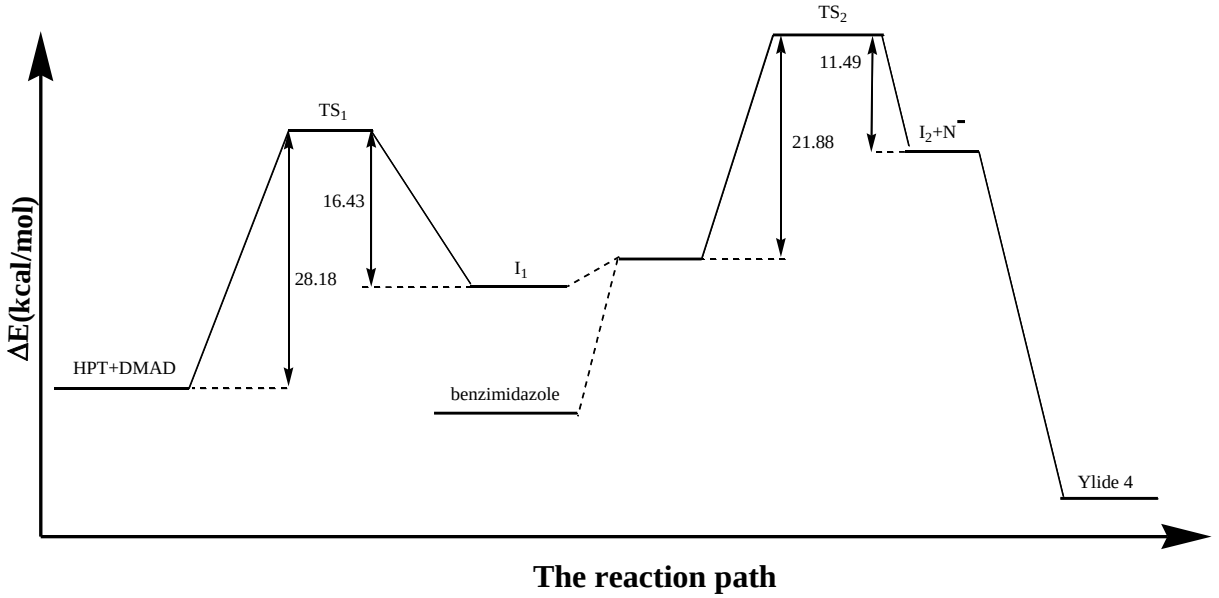

Figure 12: Based on the speculative mechanism 1 at the HF/6-31G(d,p) level of theory and extra 6-31+G(3df,3pd) basis set for P and N atoms, the total potential surface of the aforementioned reaction is calculated

Table 6 illustrates the computed activation parameters, including $\Delta G^{\neq}$, $\Delta H^{\neq}$, and $\Delta S^{\neq}$, for every step of mechanism 1 ($\Delta G^{\neq} = G_{TS} - (G_{HTP} + G_{DMAD})$, $\Delta H^{\neq} = H_{TS} - (H_{HTP} + H_{DMAD})$ and $\Delta S^{\neq} = (\Delta H^{\neq} - \Delta G^{\neq})/T$).

Table 6: The activation parameters for the $step_{1\text{-}1}$ and $step_{1\text{-}2}$ in the mechanism 1 of the reaction between **1**, **2**(Me) and **3** ($\Delta G^{\neq}$, $\Delta S^{\neq}$and $\Delta H^{\neq}$)

	$\Delta G^{\neq}$ (kcal.mol^{-1})	$\Delta S^{\neq}$ (kcal.mol^{-1}.K^{-1})	$\Delta H^{\neq}$ (kcal.mol^{-1})
$step_{1\text{-}1}(k_2)$	17.60	-0.008	15.08
$step_{1\text{-}2}(k_3)$	32.76	-0.026	25.11

The information tabulated in Table 5 revealed that the initial step (rate constant k_2) of mechanism 1 constitutes the RDS. This observation is in line with the experimental findings documented in Table 3.

Theoretical investigation into the proposed speculative mechanism. No. 2

The initial step is the same for both of proposed mechanisms 1 and 2. As for the second step, namely $step_{2\text{-}2}$ depicted in Figure 13, a concerted reaction ensues that involves N_1-H bond cleavage as well as the formation of H-O_w and N_1-C_z bonds. This progression takes place through a second transition state ($TS_{2\text{-}2}$) that adheres to a five-member ring geometry, ultimately leading to the generation of intermediate 2 (I_2).

The transition state ($TS_{2\text{-}2}$) exhibits a separation measurement of 1.06 angstrom for the breaking of the N_1-H bond, while concurrently displaying forming bond distances of 1.56 angstrom for the H-O_w bond and 1.49 angstrom for the N_1-C_z bond to generate the intermediate I_2. The presence of an imaginary frequency (1623i) within $TS_{2\text{-}2}$ substantiates its classification as a transition state. During the third step of mechanism 2, intermediate I_2 undergoes a process of conversion to form phosphorus ylide 4. This transformation occurs by passing through a third transition state ($TS_{2\text{-}3}$) that contains a four-membered ring

structure. The presence of an imaginary frequency (2349.16i) within TS_{2-3} confirms its classification as a transition state. The concerted reaction is initiated with the cleavage of the C_z-C double bond and O_w-H single bond, followed by the formation of two new bonds, including C-O_w double bonds and C_z-H single bonds. The activation energies required for each step of mechanism 2, namely the first TS_{2-1}(=TS_{1-1}), the second TS_{2-2}, and the third TS_{2-3}, were calculated using the same methodology employed for mechanism 1, which yielded values of 28.18 (k_2), 20.04 (k_3), and 78.28 (k_4) kcal.mol^{-1}, respectively. It is noteworthy that step 3, with rate constant k_4, is the rate-determining step in this process.

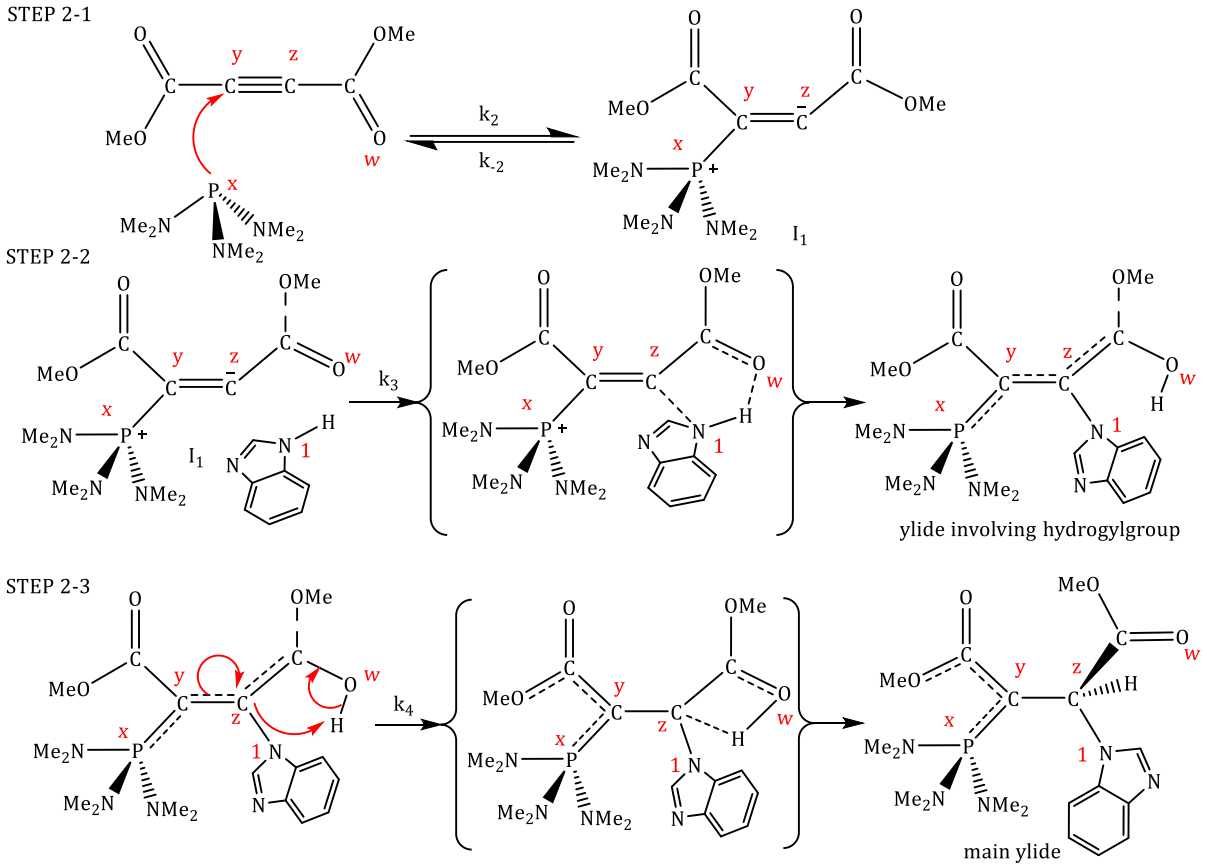

Figure 13: Generation of ylides 4 through three steps: a hypothetical proposed mechanism 2

Theoretical investigation into the proposed speculative mechanism. No. 3

Comparable to mechanisms 1 and 2's first stages, also known as $step_{1-1}$ and $step_{2-1}$, respectively, mechanism 3's $step_{3-1}$ is the first stage.

During the second stage of mechanism 3, or $step_{3-2}$, as illustrated in Figure 14, intermediate I_1 and benzimidazole engage in a concerted reaction that passes through a second transition state (TS_{3-2}). This process involves a three-membered ring, along with N_1-H bond cleavage and the formation of H-C_z and N_1-C_z bonds instantaneously. The presence of an imaginary frequency (1472i cm^{-1}) confirms TS_{3-2} as a transition state. The activation energies required for the two stages of mechanism 3 were determined to be 28.18 (k_2) and 25.71 (k_3) kcal.mol^{-1}, respectively. It is significant to note that, in line with the experimental results, step one of mechanism 3, which has a rate constant of k_2, is the RDS.

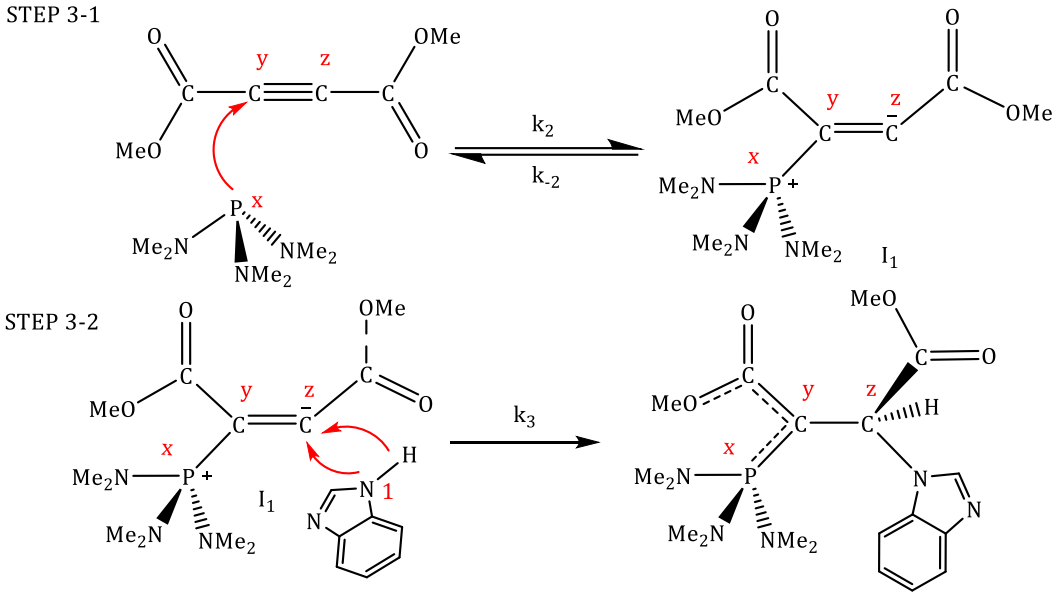

Figure 14: Generation of ylides 4 through three steps: a hypothetical proposed mechanism 3

Based on the findings of the experimental and theoretical analysis, this study presents the significant kinetics and thermodynamic parameters for the rate-limiting step of each hypothetical mechanism derived from UV-Vis experiments and quantum mechanical calculations (for three mechanisms). These parameters can be found in Table 7.

Table 7: Kinetics and thermodaynamic parameters for proposed experimental and theoretical mechanism along with rate determining step (r.d.s) at 25 °C

		r.d.s 25°C	*E*a (kcal.mol^{-1})	ΔG° (kcal.mol^{-1})	ΔH° (kcal.mol^{-1})	ΔS° (kcal.mol^{-1}.K^{-1})
Experimental [a]		k_2	45.2	-	-	-
Theoretical Mechanism	1	k_2	28.2	-17.47	-21.52	-0.014
	2	k_4	78.3	-10.12	-10.74	-0.0021
	3	k_2	28.2	-17.47	-21.52	-0.014

[a] For 1 and 2 dichloethane solvent

The results of the study indicate that theoretical mechanism 1, which corresponds exactly with the experimental kinetic mechanism, is valid for the following reasons: Firstly, the initial step in both mechanisms is the rate-determining step (as indicated in Table 7), indicating compatibility between the two mechanisms. Secondly, the second step (k_3) is a fast step (refer to Table 5), which is consistent with the experimental kinetic mechanism. On the other hand, mechanism 2, which has high activation energy (78.3 kcal.mol^{-1}) when compared to mechanisms 1 and 3, is not a plausible suggestion. In this case, the third step (k_4) is the RDS which involves an ylide containing a hydroxyl group. This compound must be transformed into the main ylide through a four-membered ring transition state (TS) with a rate constant of k_4. This process is exceedingly difficult and requires high activation energy (78.3 kcal.mol^{-1}, as indicated in Table 7 and Figure 13). Furtehrmore, because the ylide (with a hydroxyl group) in step 4 has a charge, it should be converted to the main ylide independently of solvent effects according to the concerted

mechanism. However, the experimental data show that changes in solvent polarity (high dielectric constant) accelerate the reaction. Therefore, mechanism 2 is not acceptable. In speculative mechanism 3, the second step (k_3) is the rate-determining step, which is inconsistent with the experimental results indicating that the initial step (k_2) is the rate-determining step. However, the second step (k_3) of mechanism 3 is more difficult than the second step (k_3) of mechanism 1. Therefore, mechanism 1 is considered more feasible.

Theoretical calculations for interchangeable process between the two Z-4(a, b) and E-4(a, b) isomers in the C=C bond

For reaction involving the two isomers is shown in Figures 15 and 16.

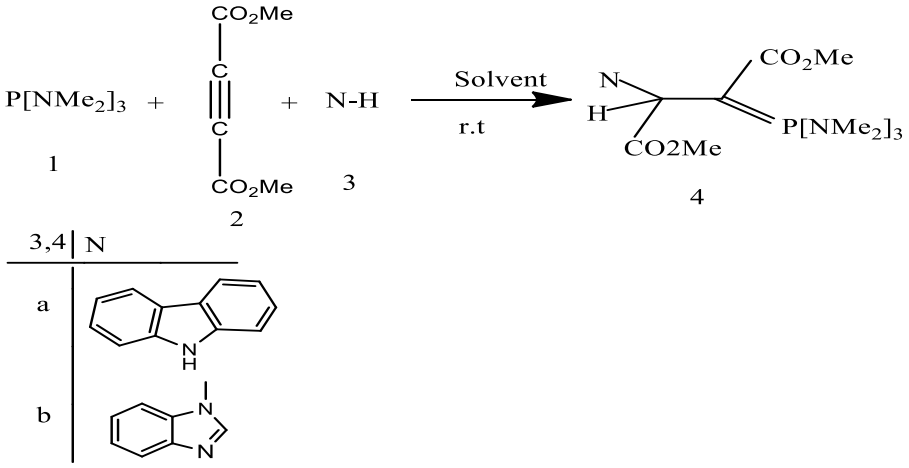

Figure 15: The reaction between compounds (1), (2. Me) and (3) for generation of phosphorous ylide **4a**-**b**

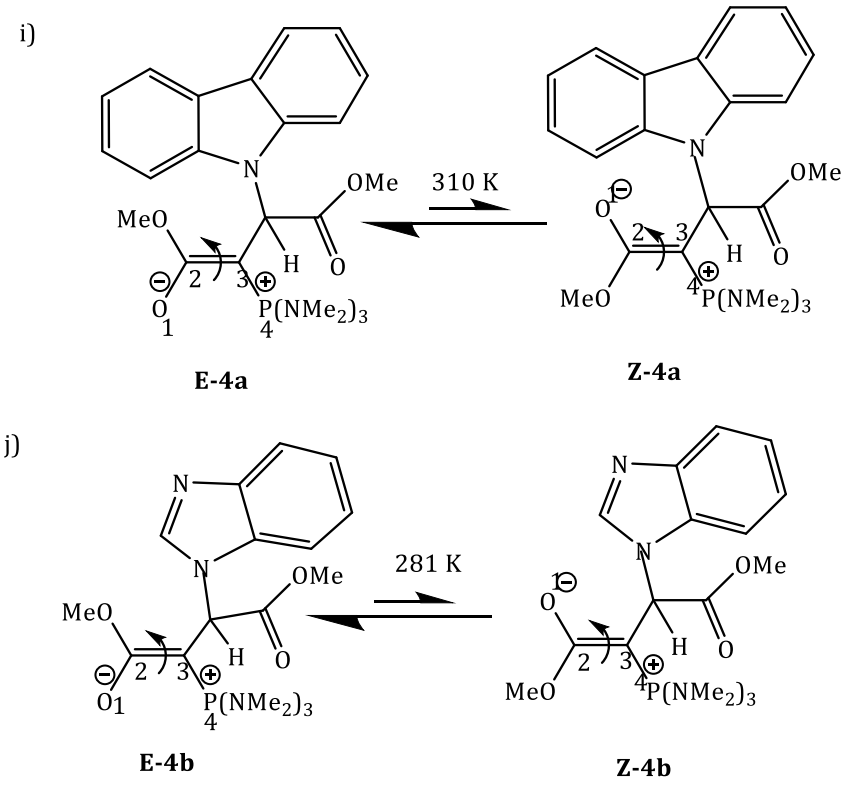

Figure 16: Interchangeable process between the two i) **E-4a** and **Z-4a** forms. j) **E-4b** and **Z-4b** rotational isomers

Their structures were optimized at the HF/6-31G (d,p) level of theory to identify the theoretical rotational energy barrier in the processes allowing the two Z- and E-isomers in ylide 4a-b to rotate interchangeably. Next, the relative energy was plotted against the dihedral angle ($O_1C_2C_3P_4$, as demonstrated in Figure 16), which is presented in Figure 17. The plot in Figure 17 was generated using a scanning method at the HF/6-31G(d,p) level of theory, and each point was fully optimized in the relevant figures. As indicated in Figure 17, only one transition state (TS) appears at the maximum point of this plot (i and j in Figure 17).

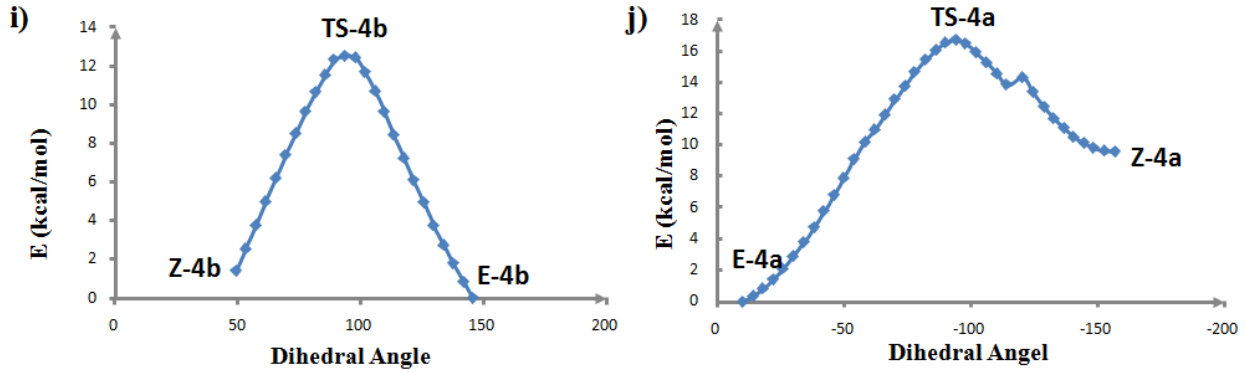

Figure 17: i) The dihedral angels of $O_1C_2C_3P_4$ and the relative energy of phosphorus ylide 4a. **j)** The dihedral angels of $O_1C_2C_3P_4$ and the relative energy of phosphorus ylide 4b

All of the points (Z, TS, and E) in Figure 17 (i, j) have corresponding structures, which are shown in Figures 18 and 19.

Based on theoretical computations and acquired data from Figures 17, 18, and 19 regarding the synthesized ylides 4a and 4b, the free Gibbs rotational energy barrier $\Delta G^{\neq}$, $\Delta H^{\neq}$, and $\Delta S^{\neq}$ encircling the carbon-carbon double bond have been calculated for all temperatures scrutinized. These outcomes have been appraised with the experimental data procured by dynamic ^{1}H-NMR data [11] (Tables 8 and 9). Furthermore, the influence of a solvent medium ($CDCl_3$) has been scrutinized to compare the gas and liquid mediums. The resulting data has been amassed in Tables 8 and 9.

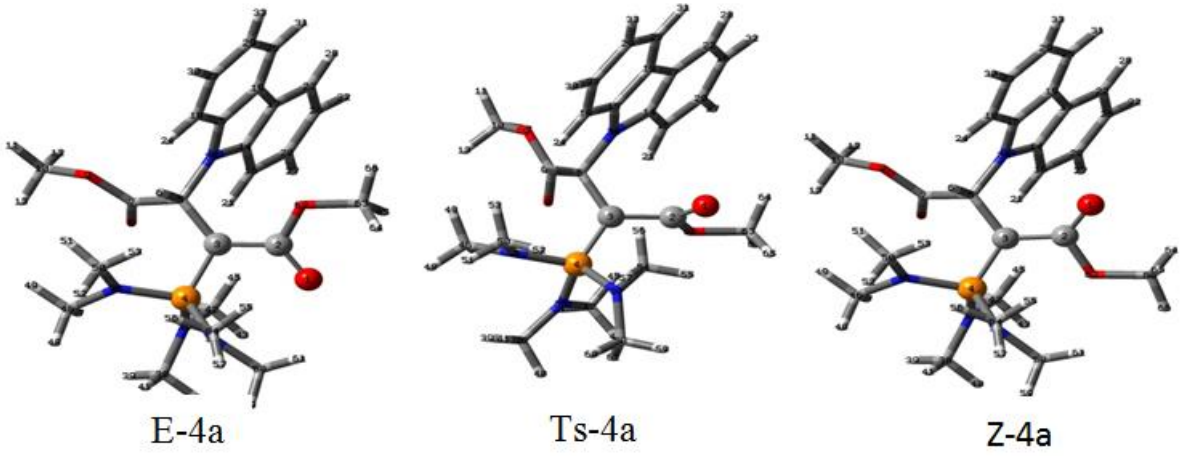

Figure 18: The scheme for the E, Z, and TS points in Figure **17i**.

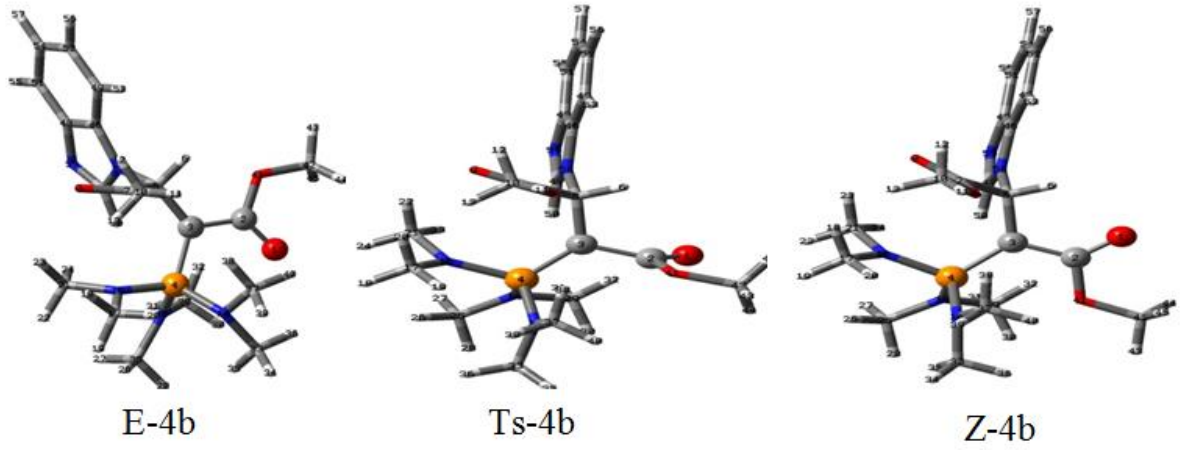

Figure 19: The scheme for the E, Z, and TS points in Figure **17j**

Table 8: Selected ^{1}H chemical shifts around the carbon-carbon double bond $(NMe_2)_3P–C\equiv C–OMe$) in ylide **4a**, a smaller molecule, were measured at 500.1(MHz, in ppm) and with activation parameters in $CDCl_3$

	$\Delta S^{\#}$ (kcal.mol^{-1}. K^{-1})	$\Delta H^{\#}$ (kcal.mol^{-1})	$\Delta G^{\#}$ (kcal.mol^{-1})	Δυ (Hz)	δ (ppm)	T_c (K)
Experimental[a]	0.006	17.71	15.65±1	25.00	5.67, 5.72	310
Theoretical[b]	-0.001	9.53	9.99	–	–	298
Theoretical[c]	-0.002	9.51	9.51	-	-	310
Theoretical[d](solvent)	-0.05	8.91	10.01			310
Theoretical[e]	-0.002	7.68	8.17			310
Theoretical[f](solvent)	-0.002	7.40	8.15	-	-	310

[a] *based on reviews of literature [34].*

[b] *The ab initio method was used to obtain data for the synthesized ylide 4a at 298 K (HF/6-31G(d,p)).*

[c] *The ab initio method was used to obtain data for the synthesized ylide 4a at 310 K (HF/6-31G(d,p)).*

[d] *The ab initio method was used to obtain data for the synthesized ylide 4a at 310 K (HF/6-31G(d,p) and solvent ($CDCl_3$)).*

[e] *The ab initio method was used to obtain data for the synthesized ylide 4a at 310 K (B3LYP/6-31G(d,p)).*

[f] *The ab initio method was used to obtain data for the synthesized ylide 4a at 310 K (B3LYP/6-31G(d,p) and solvent ($CDCl_3$)).*

Table 9: Selected 1H chemical shifts around the carbon-carbon double bond (NMe2)3P–C C–OMe) in ylide 4b, a smaller molecule, were measured at 500.1(MHz, in ppm) and with activation parameters in CDCl3

	$\Delta S^{\#}$ (kcal.mol^{-1}. K^{-1})	$\Delta H^{\#}$ (kcal.mol^{-1})	$\Delta G^{\#}$ (kcal.mol^{-1})	Δυ (Hz)	δ (ppm)	T_c (K)
Experimental[a]	-0.011	11.90	15.03±1	5.00	5.16, 5.17	281
Theoretical[b]	-0.004	19.33	25.60	–	–	298
Theoretical[c]	-0.004	19.39	19.90	-	-	281
Theoretical[d](solvent)	-0.003	19.55	20.32	-	-	281
Theoretical[e]	-0.028	18.91	18.92			281
Theoretical[f](solvent)	-0.002	16.40	17.10			281

[a] *based on reviews of literature [34].*

[b] *The ab initio method was used to obtain data for the synthesized ylide 4b at 298 K (HF/6-31G(d,p)).*

[c] *The ab initio method was used to obtain data for the synthesized ylide 4b at 281 K (HF/6-31G(d,p)).*

[d] *The ab initio method was used to obtain data for the synthesized ylide 4b at 281 K (HF/6-31G(d,p) and solvent ($CDCl_3$)).*

[e] *The ab initio method was used to obtain data for the synthesized ylide 4b at 281 K (B3LYP/6-31G(d,p)).*

[f] *The ab initio method was used to obtain data for the synthesized ylide 4b at 281 K (B3LYP/6-31G(d,p) and solvent ($CDCl_3$))*

Tables 1 and 2 indicate the Gibbs free energy values for the C=C bond at HF/6-31G (d, p) level, for compound 4a (ΔG# =10.01 kcal/mol, CDCl3as a solvent). These values exhibit reasonable agreement with the corresponding experimental data (ΔG# =15.65 kcal/mol). Conversely, at the B3LYP/6-31G (d, p) level with the same solvent, the activation parameter (ΔG# =17.1 kcal/mol) for rotation around the C=C bond of compound 4b indicates consistency with experimental observations (ΔG# =15.03 kcal/mol). This suggests that for smaller molecules (4b), the B3LYP/6-31G(d,p) level provides more accurate mechanical calculations. In contrast, the HF/6-31G(d,p) level appears to be a better option for larger molecules.

Conclusion

In summary, this article reports the primary findings resulting from the kinetics inquiry of the reactions presented in the study utilizing both experimental studies via UV-Vis spectrophotometer and theoretical studies, which are listed hereafter:

1) Experiments were conducted that involved UV-Vis methodology for kinetic evaluation, and theoretical analyses derived from the ab initio approach at both HF/6-31G (d, p) and B3LYP/6-31G (d, p) levels of theory, with the aim of obtaining greater comprehension of the reaction mechanism.

2) Based on the gathered empirical data, the initial step of the proposed experimental mechanism has been identified as the rate-determining step (k_2), and the validity of the reaction mechanism has been verified using the steady-state approximation in conjunction with the gathered experimental data.

3) The activation energy (Ea) observed to the reaction of dimethyl acetylenedicarboxylate (DMAD) and di-tert-butylacetylenedicarboxylate (tBu), carried out in the identical solvent 1,2-dichloroethane, was found to differ significantly. Specifically, the Ea for the former (2.59 $kcal.mol^{-1}$) was observed to be substantially lower than that of the latter (6.22 $kcal.mol^{-1}$).

4) Based on structural considerations, the outcomes revealed a propensity for diminished overall reaction rates in instances where bulkier and more sterically constrained alkyl groups are present, thereby accentuating the inductive impact of the dialkyl acetylenedicarboxylate structure.

5) The outcomes indicated that the rate of every reaction rose when situated in a solution of greater dielectric constant, specifically in 1,2-dichloroethane. This phenomenon can be attributed to the diverse degrees of stabilization that the solvent produces on both the reactants and the transitional state's activated complex (solvent effect).

6) To validate the suggested experimental mechanism, three hypothetical mechanisms (designated as 1, 2, and 3) have been postulated through the use of theoretical calculations. The outcomes have demonstrated that only mechanism 1, which corresponds to the experimental mechanism, is a viable and reasonable option, with the initiating step (k_2) considered as the rate-determining factor.

7) The outcomes derived from the experimentation refuted the proposed mechanism 3, asserting that the rate determining step is constituted by (k_4) and (k_3).

8) In view of theoretical data, the interchangeable process that occurs between the two rotational isomers, namely **4a**, **4b** (**4-E (a, b),** and **4-Z (a, b**)) can be characterized based on their Gibbs free energy ($\Delta G^{\#}$) values. The dynamic ^{1}H-NMR experimental data obtained at different computational levels (HF/6-31G (d, p) and B3LYP/6-31G(d,p) for 4a and 4b, respectively) indicate that the Gibbs free energy values are consistent with the theoretical data. These findings suggest that a higher basis set (B3LYP/6-31G(d,p)) provides an accurate description of smaller molecules (**4b**), whereas a lower basis set (HF/6-31G(d,p)) is suitable for larger molecules (**4a**).

Conflicts of interest

The authors state that they have no competing interests. The writing and content of this article are solely the authors' responsibility.

Disclosure Statement

No potential conflict of interest was reported by the authors.

Funding

This study did not receive any specific grant from funding agencies in the public, commercial, or not-for-profit sectors.

Authors' contributions

All authors contributed toward data analysis, drafting, and revising the paper and agreed to responsible for all the aspects of this work.

Conflict of interest

The authors declare that they have no conflicts of interest in this article.

ORCID

Younes Ghalandarzehi
https://orcid.org/0000-0002-6051-4906
Halime Kord-Tamandani
https://orcid.org/0000-0001-9823-3715

References

[**1**]. a) Mann J., Baron A., Opoku-Boahen Y., Johansson E., Parkinson G., Kelland L.R., Neidle S., A new class of symmetric bisbenzimidazole-based DNA minor groove-binding agents showing antitumor activity, *Journal of medicinal chemistry*, 2001, **44**:138 [Crossref], [Google Scholar], [Publisher]; b) Dasgupta H., Mukherjee S., ghosh P. One Pot Reductive Synthesis of Benzimidazole Derivatives from 2-Nitro Aniline and Aromatic Aldehydes Using Zn/NaHSO3 in Water Medium. *Progress in Chemical and Biochemical Research*, 2021, **4**:5 [Crossref], [Publisher]; c) John A., Ebune A., Aderemi I., Moyosore A., Idah G. Theoretical Investigation and Design of Novel Anti-proliferative Agents against Hepatocellular Carcinoma from Benzimidazole-Chalcone derivatives. *Advanced Journal of Chemistry, Section A*, 2023, **6**:92 [Crossref], [Publisher]; d) Banary H., Kolvari E., Hajiabbasi Tabar Amiri P. Surfactant-Assisted Syntheses of Benzimidazole Derivatives in Aqueous Media. *Journal of Applied Organometallic Chemistry*, 2023, **3**:134 [Crossref], [Publisher]; e) Rezayati S., Mehmannavaz M., Salehi E., Haghi S., Hajinasiri R., Afshari Sharif Abad S. Phospho Sulfonic Acid Catalyzed Synthesis of Benzimidazole, Benzoxazole and Quinoxaline Derivatives under Green Solvent at Ambient Temperature. *Journal of Sciences, Islamic Republic of Iran*, 2016, **27**:51 [Google Scholar], [Publisher];

[**2**]. a) Rajendiran V., Murali M., Suresh E., Sinha S., Somasundaram K., Palaniandavar M., Mixed ligand ruthenium (II) complexes of bis (pyrid-2-yl)-/bis (benzimidazol-2-yl)-dithioether and diimines: Study of non-covalent DNA binding and cytotoxicity, *Dalton Transactions*, 2008, 148 [Crossref], [Google Scholar], [Publisher]; b) Hakimi F., Dehghan Niri M., Banitaba S.H., Golrasan E. A facile synthesis of benzimidazole derivatives over zinc sulfide nanoparticles as heterogeneous catalyst. *Asian Journal of Green Chemistry*, 2020, **4**:239 [Crossref], [Publisher]; c) Rezaee Nezhad E., Tahmasebi R. Ionic liquid supported on magnetic nanoparticles as an efficient and reusable green catalyst for synthesis of benzimidazole derivatives under solvent and solvent-free conditions. *Asian Journal of Green Chemistry*, 2019, **3**:34 [Crossref], [Publisher]

[**3**]. Naithani P., Srivastava V., Saxena A., Barthwal J., Gupta T., Shanker K., Antiparkinsonian activity and dopamine receptor binding studies of imidazolone derivatives, *Indian journal of experimental biology*, 1990, **28**:1145 [Google Scholar], [Publisher]

[**4**]. Goudgaon N.M., Dhondiba V., Vijayalaxmi A., Synthesis and antimicrobial activity of N-1 substituted benzimidazoles. *Indian Journal of Heterocyclic Chemistry,* 2004, **13**:271 [Google Scholar], [Publisher]

[**5**]. Sperandio D., Gangloff A.R., Litvak J., Goldsmith R., Hataye J.M., Wang V.R., Shelton E.J., Elrod K., Janc J.W., Clark J.M., Highly potent non-peptidic inhibitors of the HCV NS3/NS4A serine protease, *Bioorganic & medicinal chemistry letters*, 2002, **12**:3129 [Crossref], [Google Scholar], [Publisher]

[**6**]. Ghani N.T.A., Mansour A.M., Novel palladium (II) and platinum (II) complexes with 1H-

benzimidazol-2-ylmethyl-N-(4-bromo-phenyl)-amine: Structural studies and anticancer activity, *European journal of medicinal chemistry*, 2012, **47**:399 [Crossref], [Google Scholar], [Publisher]
[**7**]. Ghani N.T.A., Mansour A.M., Palladium (II) and platinum (II) complexes containing benzimidazole ligands: Molecular structures, vibrational frequencies and cytotoxicity, *Journal of Molecular Structure*, 2011, **991**:108 [Crossref], [Google Scholar], [Publisher]
[**8**]. Mayanna S., Setty T., Effect of Benzotriazole on the dissolution of copper single crystal planes in dilute sulphuric acid, *Corrosion Science*, 1975, **15**:627 [Crossref], [Google Scholar], [Publisher]
[**9**]. Wittig G., from diyls to ylides to my idyll, *Science*, 1980, **210**:600 [Crossref], [Google Scholar], [Publisher]
[**10**]. Kolodiazhnyi O.I., Methods of preparation of C-substituted phosphorus ylides and their application in organic synthesis, *Russian chemical reviews*, 1997, **66**:225 [Google Scholar], [Publisher]
[**11**]. Pietrusiewicz K.M., Zablocka M., Preparation of scalemic P-chiral phosphines and their derivatives, *Chemical reviews*, 1994, **94**:1375 [Crossref], [Google Scholar], [Publisher]
[**12**]. Bokach N.A., Kukushkin V.Y., Haukka M., Fraústo da Silva J.J., Pombeiro A.J., Pop-the-Cork strategy in synthetic utilization of imines: stabilization by complexation and activation via liberation of the ligated species, *Inorganic chemistry*, 2003, **42**:3602 [Crossref], [Google Scholar], [Publisher]
[**13**]. Kolodiazhnyi O.I., C-element-substituted phosphorus ylids, *Tetrahedron*, 1996, **52**:1855 [Crossref], [Google Scholar], [Publisher]
[**14**]. Wagner G., Pakhomova T.B., Bokach N.A., Fraústo da Silva J.J., Vicente J., Pombeiro A.J., Kukushkin V.Y., Reduction of (imine) Pt (IV) to (imine) Pt (II) complexes with carbonyl-stabilized phosphorus ylides, *Inorganic chemistry*, 2001, **40**:1683 [Crossref], [Google Scholar], [Publisher]
[15]. Asghari S., Habibi A.K., Triphenylphosphine-catalyzed synthesis of stable, functionalized 2H-oxetes, *Phosphorus, Sulfur, and Silicon*, 2005, **180**:2451 [Crossref], [Google Scholar], [Publisher]
[**16**]. Yavari I., Asghari S., Esmaili A.A., Vinyltriphenylphosphonium salt-mediated new synthesis of functionalized maleimides, *Journal of Chemical Research*, 1999, **23**:234 [Crossref], [Google Scholar], [Publisher]
[**17**]. Galariniotou E., Fragos V., Makri A., Litinas K.E., Nicolaides D.N., Synthesis of novel pyridocoumarins and benzo-fused 6-azacoumarins, *Tetrahedron*, 2007, **63**:8298 [Crossref], [Google Scholar], [Publisher]
[**18**]. Kolodiazhnyi O.I., Phosphorus ylides: chemistry and applications in organic synthesis, *John Wiley & Sons*, 2008 [Google Scholar], [Publisher]
[**19**]. Asghari S., Tajbakhsh M., Taghipour V., A facile route to N-acetyl α, β-unsaturated γ-lactam derivatives using ethyl acetamidocyanoacetate and dialkyl acetylenedicarboxylate in the presence of triphenylphosphine, *Tetrahedron Letters*, 2008, **49**:1824 [Crossref], [Google Scholar], [Publisher]
[**20**]. Evans L.A., Griffiths K.E., Guthmann H., Murphy P.J., Intramolecular Wittig reactions with esters utilising triphenylphosphine and dimethyl acetylenedicarboxylate, *Tetrahedron Letters*, 2002, **43**:299 [Crossref], [Google Scholar], [Publisher]
[**21**]. Habibi-Khorassani S.M., Maghsoodlou M.T., Ebrahimi A., Farahani F.V., Mosaddeg E., Kazemian M.A., Dynamic 1H NMR study around the heteroaryl–carbon and carbon–carbon single bonds and also around carbon–carbon double bond in a particular phosphorous ylide involving a 2-methyl indole, *Tetrahedron Letters*, 2009, **50**:3621 [Crossref], [Google Scholar], [Publisher]
[**22**]. Nicolaou K., Härter M.W., Gunzner J.L., Nadin A., The Wittig and related reactions in natural product synthesis, *Liebigs Annalen*, 1997, **1997**:1283 [Crossref], [Google Scholar], [Publisher]
[**23**]. Okubo T., Maeda Y., Kitano H., Inclusion process of ionic detergents with cyclodextrins as studied by the conductance stopped-flow method, *The Journal of Physical Chemistry*, 1989, **93**:3721 [Crossref], [Google Scholar], [Publisher]
[**24**]. Maghsoodlou M., Marandi G., Habibi-Khorasani S.M., saghatforoush L., Aminkhani A.,

Kabiri R., *Indian J. Chem. B*, 2008, **47**:1151 [Google Scholar]

[**25**]. Shahraki M., Habibi-Khorassani S.M., Ebrahimi A., Maghsoodlou M., Ghalandarzehi Y., Intramolecular hydrogen bonding in chemoselective synthesized 2-substituted pyrrole stable phosphorus ylide: GIAO, AIM, and NBO approaches, *Structural Chemistry*, 2013, **24**:623 [Crossref], [Google Scholar], [Publisher]

[**26**]. Ziyaadini M.M., MT; Hazeri N., Habibi-Khorassani S.M., *Monatshefte fur Chememie*, 2012, **143**:1681 [Google Scholar]

[**27**]. Gordon M., Jensen J., Koseki S., Matsunaga, N., Nguyen K., Su S., Windus T., Partially based on us gamess version 6 jun 1999,* US gamess versions 6 sep 2001 and 12 dec 2003* from iowa state university* mw schmidt, kk baldridge, ja boatz, st elbert, *Journal of Computational Chemisry*, 1993, **14**:1347 [Google Scholar]

[**28**]. Asheri O., Habibi-Khorassani S.M., Shahraki M., A Study on the Kinetics and Mechanism of the One-Pot Formation of 3, 4, 5-Substituted Furan-2 (5 H)-Ones in the Presence of Lactic Acid: Effect of Different Substituents, *Progress in Reaction Kinetics and Mechanism*, 2018, **43**:286 [Crossref], [Google Scholar], [Publisher]

[**29**]. Asheri O., Shahraki M., Habibi-Khorassani S.M., One-Pot Multicomponent Synthesis of 2H-Chromene Derivative, Kinetics, and Thermodynamic Studies Using a Stopped-Flow Technique in Combination with Theoretical Computation Methods, *Polycyclic Aromatic Compounds*, 2020, **40**:714 [Crossref], [Google Scholar], [Publisher]

[**30**]. Darijani M., Shahraki M., Habibi-Khorassani S.M., Theoretical study on the mechanism and kinetics of the formation β-carotene epoxides from the oxidative degradation of β-carotene, *Food Chemistry*, 2022, **389**:133082 [Crossref], [Google Scholar], [Publisher]

[**31**]. Engel R., *Synthesis of carbon-phosphorus bonds*. CRC press. 2003 [Google Scholar], [Publisher]

[32]. Schwartz L.M., Gelb R.I., Alternative method of analyzing first-order kinetic data, *Analytical Chemistry*, 1978, **50**:1592 [Crossref], [Google Scholar], [Publisher]

[**34**]. Tregloan P., Laurence G., A precision conductance apparatus for studying fast ionic reactions in solution, *Journal of Scientific Instruments*, 1965, **42**:869 [Google Scholar], [Publisher]

[**35**]. Petersson A., Bennett A., Tensfeldt T.G., Al-Laham M.A., Shirley W.A., Mantzaris J., A complete basis set model chemistry. I. The total energies of closed-shell atoms and hydrides of the first-row elements, *The Journal of Chemical Physics*, 1988, **89**:2193 [Crossref], [Google Scholar], [Publisher]

[3**6**]. Petersson G., Al-Laham M.A., A complete basis set model chemistry. II. Open-shell systems and the total energies of the first-row atoms, *The Journal of Chemical Physics*, 1991, **94**:6081 [Crossref], [Google Scholar], [Publisher]

[**37**]. Gonzalez C., Schlegel H.B., An improved algorithm for reaction path following, *The Journal of Chemical Physics*, 1989, **90**:2154 [Crossref], [Google Scholar], [Publisher]

[**38**]. Becke A.D., Density-functional exchange-energy approximation with correct asymptotic behavior, *Physical review A*, 1988, **38**:3098 [Crossref], [Google Scholar], [Publisher]

[**39**]. Lee C., Yang, W., Parr R.G., Development of the Colle-Salvetti correlation-energy formula into a functional of the electron density, *Physical review B*, 1988, **37**:785 [Crossref], [Google Scholar], [Publisher]

HOW TO CITE THIS ARTICLE

Younes Ghalandarzehi*, Halime Kord-Tamandani. Experimental and Theoretical Study on the Mechanism and Kinetics of the Reaction between Hexamethyl Phosphorous Triamide and Dialkyl Acetylenedicarboxylates in the Presence of Benzimidazole. *Chem. Methodol.*, 2023, 7(10) 776-798

DOI: https://doi.org/10.48309/chemm.2023.412486.1714

URL: https://www.chemmethod.com/article_182032.html